Classical and quantum distinctions between weak and strong coupling

2016 Eur. J. Phys. 37 025802

(http://iopscience.iop.org/0143-0807/37/2/025802)

IOP Publishing European Journal of Physics
Eur. J. Phys. **37** (2016) 025802 (15pp) doi:10.1088/0143-0807/37/2/025802

Classical and quantum distinctions between weak and strong coupling

Said Rahimzadeh-Kalaleh Rodriguez

[1] Center for Nanophotonics, FOM Institute AMOLF, c/o Philips Research Laboratories, High Tech Campus 4, 5656 AE Eindhoven, The Netherlands
[2] Laboratoire de Photonique et de Nanostructures, LPN/CNRS, Route de Nozay, F-91460 Marcoussis, France

E-mail: said.rodriguez@lpn.cnrs.fr

Received 12 October 2015, revised 4 December 2015
Accepted for publication 15 January 2016
Published 29 January 2016

Abstract

Coupled systems subject to dissipation exhibit two different regimes known as weak coupling and strong coupling. Two damped coupled harmonic oscillators (CHOs) constitute a model system where the key features of weak and strong coupling can be identified. Several of these features are common to classical and quantum systems, as a number of quantum-classical correspondences have shown. However, the condition defining the boundary between weak and strong coupling is distinct in classical and quantum formalisms. Here we describe the origin of two widely used definitions of strong coupling. Using a classical CHO model, we show that energy exchange cycles and avoided resonance crossings signal the onset of strong coupling according to one criterion. From the classical CHO model we derive a non-Hermitian Hamiltonian describing open quantum systems. Based on the analytic properties of the Hamiltonian, we identify the boundary between weak and strong coupling with a different feature: a non-Hermitian degeneracy known as the exceptional point. For certain parameter ranges the classical and quantum criterion for strong coupling coincide; for other ranges they do not. Examples of systems in strong coupling according to one or another criterion, but not both, are illustrated. The framework here presented is suitable for introducing graduate or advanced undegraduate students to the basic properties of strongly coupled systems, as well as to the similarities and subtle differences between classical and quantum descriptions of coupled dissipative systems.

Keywords: coupled oscillators, strong coupling, exceptional point, avoided resonance crossing

(Some figures may appear in colour only in the online journal)

1. Introduction

Studies of energy transfer are at the foundation of physics. Two damped coupled harmonic oscillators (CHOs) constitute an illustrative system where the interplay between energy exchange and dissipation can be recognized. The CHOs exchange energy between them via a coupling spring, while they each loose energy to their surroundings via friction. Consequently, qualitatively distinct behaviour emerges when one of these processes dominates. In this light, one of the most important distinctions in the physics of coupled dissipative systems is made: weak versus strong coupling. For two CHOs, weak and strong coupling are commonly identified in three contexts: (i) the dynamics is governed by exponential decay or energy exchange cycles; (ii) the steady-state spectrum of the driven system displays a single resonance or two split peaks; (iii) the eigenfrequencies of the CHOs cross or anti-cross as the frequency difference between the bare oscillators transits through zero. Naturally, the analysis of dynamics, steady-state spectra, and eigenvalues also constitute the main arena of the dissipative two-state quantum model [1]. Despite the many parallels between classical and quantum descriptions of coupled dissipative systems [2], two distinct criteria for strong coupling are widespread.

One criterion for strong coupling relies on the energy exchange rate exceeding all loss rates. Novotny quotes a tighter variant of this criterion: 'to observe strong coupling, the frequency splitting [$\propto$ coupling strength] needs to be larger than the sum of the linewidths [$\propto$ loss rates]' [3]. The spectrum of a driven CHO system under this condition displays two split resonances provided that the driving force does not excite only one eigenmode of the system. Hence, in a similar spirit Törmä and Barnes defined the coupling regime based on whether two split peaks are visible in the spectrum (strong coupling) or not (weak coupling) [4].

A second (different) criterion for strong coupling involves the energy exchange rate exceeding the difference between the loss rates rather than their individual magnitudes or their sum (see e.g. Andreani [5] or Laussy *et al* [6]). This second criterion implies that two identical oscillators with arbitrarily high losses are strongly coupled for any non-zero energy exchange rate. If the energy exchange rate is much less than the loss rates, the strongly coupled system is incapable of exhibiting energy exchange cycles or split peaks in the spectrum. Nevertheless, two levels anti-cross provided that the difference between their loss rates is sufficiently small compared to their energy exchange rate.

The two criteria described above give the same result for many systems deep into the strong or weak coupling regimes. However, intermediate regimes exist where a given system can fulfill one condition for strong coupling but not the other. While the first (second) condition for strong coupling is more often encountered in classical (quantum) formalisms, no particular axiom of classical or quantum mechanics holds any of these criteria above the other. As we will see, it is simply the analysis of different features which gives rise to distinct criteria. Understanding these differences is crucial for assessing the characteristic time scales of a system. This understanding is also relevant in the context of many quantum-classical correspondences, where CHOs have played a prominent role [3, 7–21]. Another motivation for distinguishing between weak and strong coupling of CHOs is related to the interpretation of experiments: CHOs are widely used to analyse experimental data based on a best-fit approach (see for example [22–28] for a far-from exhaustive list). A distinction between weak and strong coupling is necessary to determine whether the constituents of the coupled system merely perturb each other, or their mutual influence is so strong that their individuality is lost.

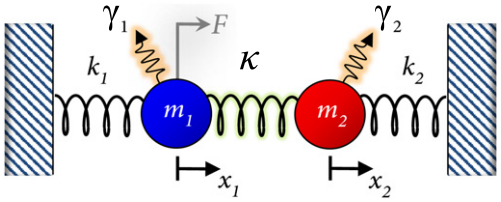

Figure 1. Two coupled harmonic oscillators. $\gamma_{1,2}$ are the loss rates, $\sqrt{k_{1,2}/m_{1,2}}$ are the eigenfrequencies of the bare oscillators, κ is the coupling spring constant, $x_{1,2}$ are the displacements from equilibrium, and F is a driving force (see text).

Here we demonstrate the different features defining the boundary between weak and strong coupling in classical and quantum frameworks. We study the classical CHO dynamics in section 2 and the steady-state spectra in section 3. Therein, we find a transition from weak to strong coupling evidenced by the onset of energy exchange cycles and frequency splitting between the CHOs. In section 4 we map the classical CHO model to the two-state non-Hermitian Hamiltonian (NHH) describing open quantum systems. The NHH has a complex energy spectrum, the imaginary part of which represents the losses. The discussion is suitable for introducing students to the non-Hermitian quantum framework. This is becoming increasingly relevant since NHHs have proven to model several physical systems more faithfully than their Hermitian counterparts [29–34]. Amongst the most remarkable features of NHHs lies a non-Hermitian degeneracy known as the exceptional point (EP) [29, 32]. In section 4 we explain the origin of the EP and its relation to the second distinction between weak and strong coupling. More generally, the derivation of a two-state NHH from the equations of motion of two damped CHOs constitutes an insightful exercise whereby students can recognize links between first-order perturbation theory and the intuitive physics of coupled oscillators. In this way, two key elements of the physics curriculum encountered in introductory quantum and classical mechanics courses can be presented in a unified framework. Consequently, students will be able to appreciate a wide range of seemingly abstract quantum phenomena from the classical perspective of coupled oscillators, while requiring only a basic knowledge of linear algebra, ordinary differential equations, and complex analysis.

2. Dynamics of CHOs

We first study the dynamics of two damped CHOs as illustrated in figure 1. In the absence of any driving force ($F = 0$), the equations of motion are

$$\begin{aligned} \ddot{x_1} + \gamma_1\dot{x_1} + \omega_1^2 x_1 - \Omega^2 x_2 = 0, \\ \ddot{x_2} + \gamma_2\dot{x_2} + \omega_2^2 x_2 - \Omega^2 x_1 = 0. \end{aligned} \tag{1}$$

x_j ($j = 1, 2$) is the displacement from equilibrium of the jth oscillator, which has an uncoupled eigenfrequency $\omega_j = \sqrt{k_j/m_j}$ and a loss rate γ_j. Let us first consider two identical oscillators: $m_1 = m_2 = m$, $k_1 = k_2 = k$, $\omega_1 = \omega_2 = \omega_0$ and $\gamma_1 = \gamma_2 = \gamma$. The oscillators are coupled at a rate $\Omega = \sqrt{\kappa/m}$, where κ is the stiffness constant of the middle spring. We focus on underdamped oscillators ($\gamma/2 < \omega_0$) which are best suited for distinguishing between weak and strong coupling. We refer to [35] for the overdamped ($\gamma/2 > \omega_0$) case and the corresponding quantum-classical correspondence.

We are interested in the time-evolution of the total energy in the oscillators when one of the oscillators is initially displaced from equilibrium, i.e., $x_1(0) \neq 0$ and $x_2 = 0$. We can solve this problem numerically in matrix form using the state-space representation. For this purpose, the two second order differential equations (equation (1)) are reduced to four first order differential equations. The state variables representing the system are

$$\begin{aligned} q_1 &= x_1, \\ q_2 &= \dot{x}_1, \\ q_3 &= x_2, \\ q_4 &= \dot{x}_2 . \end{aligned} \tag{2}$$

These variables form the state vector $\mathbf{q}$, whose time-evolution obeys the following matrix differential equation:

$$\begin{bmatrix} \dot{q}_1 \\ \dot{q}_2 \\ \dot{q}_3 \\ \dot{q}_4 \end{bmatrix} = \begin{bmatrix} 0 & 1 & 0 & 0 \\ -\omega_1^2 & -\gamma_1 & \Omega^2 & 0 \\ 0 & 0 & 0 & 1 \\ \Omega^2 & 0 & -\omega_2^2 & -\gamma_2 \end{bmatrix} \begin{bmatrix} q_1 \\ q_2 \\ q_3 \\ q_4 \end{bmatrix}. \tag{3}$$

We solve equation (3) numerically, setting $\omega_0 = 1$ rad s^{-1} and $\gamma = 10^{-3}\omega_0$. We calculate the total energy in oscillators 1 and 2 given by the sum of the kinetic and potential energies, $T_{1,2}$ and $V_{1,2}$, respectively. In terms of the state variables, $T_1 + V_1 = \frac{mq_2^2}{2} + \frac{kq_1^2}{2}$ and $T_2 + V_2 = \frac{mq_4^2}{2} + \frac{kq_3^2}{2}$.

In figure 2 we plot $T_{1,2} + V_{1,2}$ as a function of the dimensionless time constant $\Omega^2 t/(2\pi\omega_0)$ for three values of the ratio $\Omega^2/\omega_0\gamma$. When $\Omega^2 < \omega_0\gamma$, loss dominates over energy exchange. An example is shown in figure 2(a), where $\Omega^2/\omega_0\gamma = 0.5$. The initial energy stored in oscillator 1 (blue line) is dissipated before it can be transferred to oscillator 2 (red line). The dynamics is qualitatively similar for $\Omega = 0$ (not shown), where the total energy in oscillator 1 decays as $e^{-2\gamma t}$ (black dotted line). Hence, the weak coupling simply exerts a perturbative effect on the exponential energy decay of the excited CHO.

A different regime arises when $\Omega^2 > \omega_0\gamma$. We plot the dynamics for $\Omega^2/\omega_0\gamma = 1.1$ in figure 2(c), and for $\Omega^2/\omega_0\gamma = 3$ in figure 2(e). In figure 2(c) we observe a single cycle of energy exchange between the CHOs, while in figure 2(e) we observe multiple cycles. The observation of energy exchange cycles indicates that the CHOs transfer energy between them faster than they each dissipate energy. The observation of this effect is therefore often associated with the strong coupling regime. It is noteworthy that, within the classical formalism, observing energy exchange cycles requires initially displacing one of the oscillators from its equilibrium position. This means that energy needs to be externally fed into the system. According to quantum theory, this needs not be the case; an atom in a cavity can exchange energy with the vacuum field [36].

Figure 2 sheds light on a smooth boundary between weak and strong coupling at $\Omega^2/\omega_0\gamma \approx 1$. Note that for $\gamma_1 = \gamma_2 = \gamma$ we have $\Omega^2/\omega_0\gamma = 2\Omega^2/\omega(\gamma_1 + \gamma_2)$. Hence, the above definition of strong coupling is sometimes expressed in terms of the sum of the loss rates [3]. While the sum of the loss rates is a decisive factor for observing energy exchange cycles, the difference between the loss rates is not. Consider that $|\gamma_1 - \gamma_2| = 0$ for all three cases in figure 2, yet a significantly different amount of energy exchange is observed for each case. Thus, qualitatively distinct behaviour emerges even though the difference between the loss rates remains unchanged. In section 4 we will discuss the relevance of the quantity $|\gamma_1 - \gamma_2|$. By analysing different features, we will show that the value of $|\gamma_1 - \gamma_2|$ compared to

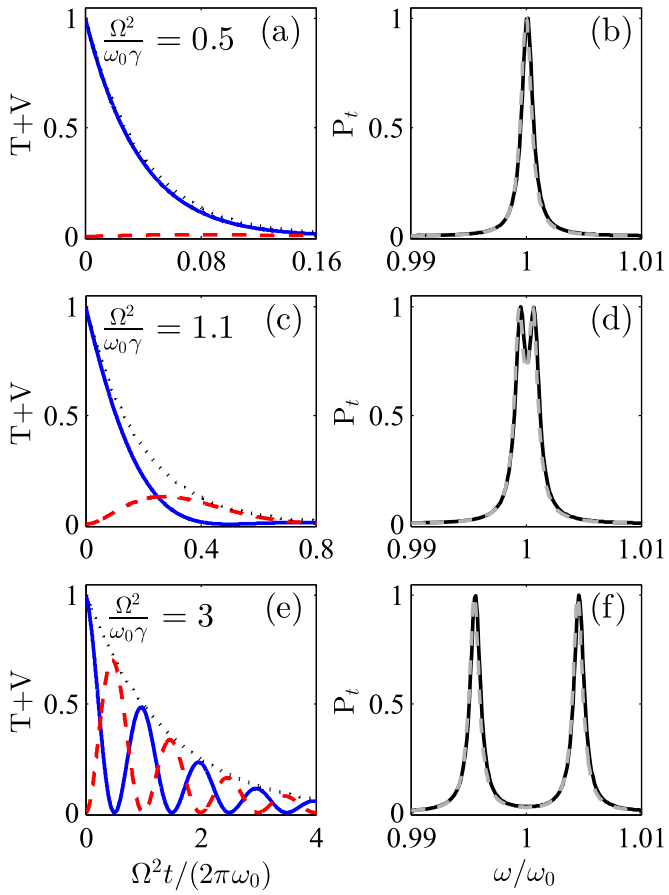

Figure 2. (a), (c) and (e) show the time evolution of the total energy (kinetic T plus potential V) in two coupled harmonic oscillators. Ω is the coupling rate, γ is the loss rate, and ω_0 is the eigenfrequency of the bare oscillators. The blue solid line is the energy in oscillator 1, the red dashed line is the energy in oscillator 2, and the dotted black line is $e^{-2\gamma t}$. In (b), (d) and (f) the black solid line is the time-integrated dissipated power by both oscillators. The overlying grey dashed line is the steady-state dissipated power by both oscillators when only one oscillator is driven by a time-harmonic force.

the value of Ω can serve to define the boundary between two distinct regimes also known as weak coupling and strong coupling.

Next we analyse the time-integrated power spectrum of the undriven initially excited CHOs. The frequency-dependence of the jth oscillator's displacement from equilibrium is obtained by Fourier-transforming its time-dependent displacement from equilibrium, viz

$$X_j(\omega) = \frac{1}{\sqrt{2\pi}} \int_{-\infty}^{\infty} x_j(t) \mathrm{e}^{-\mathrm{i}\omega t} \mathrm{d}t. \tag{4}$$

The time-integrated dissipated power spectrum is given by

$$P_j(\omega) = \omega_j^2 \gamma_j \, |X_j(\omega)|^2. \tag{5}$$

In figures 2(b), (d) and (f) we show as black solid lines the total absorbed power spectrum $P_t = P_1 + P_2$ for the corresponding time-traces in figures 2(a), (c) and (e). We normalize each

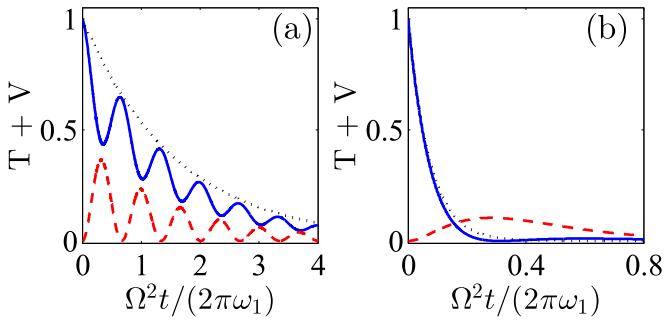

Figure 3. Time evolution of the total energy in two coupled harmonic oscillators with unequal eigenfrequencies in (a) and unequal loss rates in (b). For both plots $\omega_1 = 1$ rad s^{-1} and $\Omega_1 = 0.1$ rad m^{-1}. In (a): $\omega_2 = 0.989$ rad s^{-1} and $\gamma_1 = \gamma_2 = 1$ mrad s^{-1}. In (b) $\omega_2 = \omega_1$, $\gamma_1 = 22$ mrad s^{-1} and $\gamma_2 = 1$ mrad s^{-1}.

spectrum because we are interested in qualitative behaviour only. The spectra show the frequency splitting of a single resonance into two resonances as the coupling strength increases. This effect is often referred to as 'Rabi splitting' or 'Autler-Townes splitting', and it is regarded as the spectral signature of the transition to strong coupling. The split peaks are centered at the eigenfrequency of the bare (identical) oscillators.

In addition to the condition $\Omega^2/\omega_0\gamma \gtrsim 1$, observing energy exchange cycles requires that the initial conditions do not match an eigenmode of the system. The CHO eigenmodes involve the combined harmonic motion of the two oscillators in phase (symmetric mode) or π-dephased (anti-symmetric mode). These modes are excited for the initial conditions $x_1(0) = x_2(0) \neq 0$ and $x_1(0) = -x_2(0) \neq 0$, respectively. If an eigenmode is directly excited, the strong coupling dynamics is governed by exponential energy decay, as in weak coupling. The corresponding power spectrum displays a single resonance peak shifted from ω_0 by an amount proportional to Ω. The shift is to lower frequencies when the symmetric mode is excited, and to higher frequencies when the anti-symmetric mode is excited.

Notice in figure 2(e) that the CHOs undergo complete energy exchange at integer multiples of the time constant $\Omega^2 t/(2\pi\omega_0)$. This changes when the oscillators are detuned, as we now show. We consider the dynamics of CHOs with unequal eigenfrequencies in figure 3(a), and with unequal loss rates in figure 3(b). The rates used in the calculations are reported in the figure caption; their choice will be clarified below. Figure 3(a) shows that energy exchange cycles persist despite the detuning $\omega_1 - \omega_2 = 11$ mrad s^{-1}. In other words, the oscillators undergo exchange energy cycles even though their eigenfrequencies are significantly different. However, in contrast to the zero-detuning case where $\omega_1 = \omega_2$ (e.g. figure 2(e)), the initially excited oscillator stores more energy than its coupled partner at all times. For much greater detunings energy exchange cycles vanish and the dynamics resembles that of weak coupling instead. Figure 3(b) displays roughly a single cycle of energy exchange between CHOs with $(\gamma_1 - \gamma_2)/2 = 11.5$ mrad s^{-1}. The behaviour in this case is similar to that in figure 2(b), where the oscillators had equal loss rates and they were just above the onset of strong coupling. Notice in particular that oscillator 2 (red line) receives a significant fraction of the energy from oscillator 1 (blue line), which contrasts with the weak coupling scenario depicted in figure 2(a). Thus, the oscillators undergo significant energy exchange even though their loss rates are rather different.

In preparation for section 4, let us evaluate for all systems in figures 2 and 3 the dimensionless quantity $\Omega^2/\omega_m\Delta$, whose relevance will be clarified further ahead.

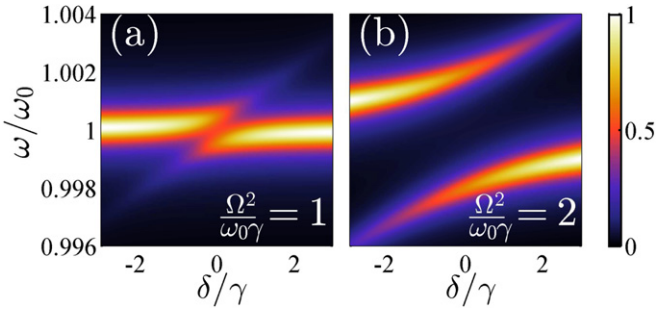

Figure 4. Total power absorbed in steady-state by two coupled harmonic oscillators with variable frequency detuning δ for two different values of $\Omega^2/\omega_0\gamma$ (see insets). In both plots, only the first oscillator with fixed eigenfrequency ω_0 is driven by a harmonic force with frequency ω.

$\Delta = (\omega_1 - \omega_2) - \mathrm{i}(\gamma_1 - \gamma_2)/2$ is the complex detuning of the bare oscillators and $\omega_m = (\omega_1 + \omega_2)/2$ is their mean eigenfrequency. Since $\Delta = 0$ for all systems in figure 2, $\Omega^2/\omega_m\Delta = \infty$. Therefore, the quantity $\Omega^2/\omega_m\Delta$ does not in general distinguish between systems that exchange energy efficiently (e.g. figure 2(e)) and those that do not (e.g. figure 2(a)). Conversely, figures 3(a) and (b) illustrate two systems for which $\Omega^2/\omega_m\Delta < 1$ yet significant energy exchange cycles are visible. In particular, for the calculation in figures 3(a) we set $\Omega^2/\omega_m\Delta = \Omega^2/\omega_m(\omega_1 - \omega_2) = 0.91$, while for figure 3(b) we set $\Omega^2/\omega_m\Delta = 2\Omega^2/\omega_m(\gamma_1 - \gamma_2) = 0.95$. The significance of these cases will be discussed in section 4, where we derive a different condition for strong coupling based on $\Omega^2/\omega_m\Delta \geqslant 1$.

3. Driven-dissipative CHOs

In this section we analytically calculate the steady-state power dissipated by a driven system of CHOs. We first consider the excitation of oscillator 1 only. The oscillator is driven by a harmonic force of amplitude per unit mass F and frequency ω. Thus, we add the term $F\mathrm{e}^{-\mathrm{i}\omega t}$ to the right-hand side of the top equation (1). Inserting the ansatz $x_j(t) = x_j^0\mathrm{e}^{-\mathrm{i}\omega t}$ in equation (1), we obtain the following matrix equations describing the driven-dissipative CHOs:

$$\begin{bmatrix} \omega_1^2 - \omega^2 - \mathrm{i}\gamma_1\omega & -\Omega^2 \\ -\Omega^2 & \omega_2^2 - \omega^2 - \mathrm{i}\gamma_2\omega \end{bmatrix}\begin{bmatrix} x_1 \\ x_2 \end{bmatrix} = \begin{bmatrix} F\mathrm{e}^{-\mathrm{i}\omega t} \\ 0 \end{bmatrix}. \tag{6}$$

Equation (6) has the form $\mathbf{Zx} = \mathbf{F}$. Rearranging as $\mathbf{x} = \mathbf{Z}^{-1}\mathbf{F}$ leads to

$$\begin{bmatrix} x_1 \\ x_2 \end{bmatrix} = \frac{1}{|\mathbf{Z}|}\begin{bmatrix} \omega_2^2 - \omega^2 - \mathrm{i}\gamma_2\omega & \Omega^2 \\ \Omega^2 & \omega_1^2 - \omega^2 - \mathrm{i}\gamma_1\omega \end{bmatrix}\begin{bmatrix} F\mathrm{e}^{-\mathrm{i}\omega t} \\ 0 \end{bmatrix}, \tag{7}$$

with $|\mathbf{Z}| = (\omega_1^2 - \omega^2 - \mathrm{i}\omega\gamma_1)(\omega_2^2 - \omega^2 - \mathrm{i}\omega\gamma_2) - \Omega^4$. In steady-state, the power dissipated by the jth oscillator at the driving frequency ω is $P_j = \omega^2\gamma_j\,|x_j(\omega)|^2$.

In figures 2(b), (d) and (f) we plot as grey dashed lines the total steady-state dissipated power spectrum $P_t = P_1 + P_2$ calculated for the same model parameters used to calculate the dynamics in figures 2(a), (c) and (e). We find an excellent agreement between the steady-state and the time-integrated dynamical response (black lines) of the system. The criterion for strong coupling is therefore identical.

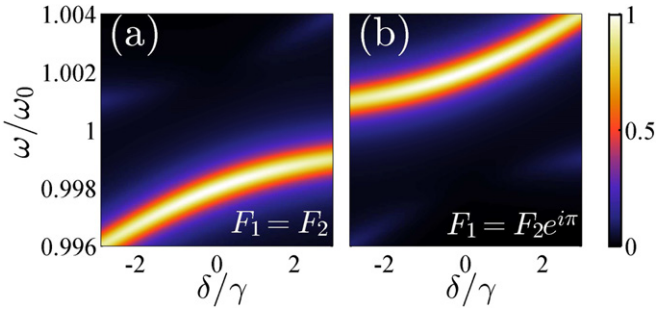

Figure 5. Total power absorbed in steady-state by two coupled harmonic oscillators with $\Omega^2/\omega\gamma = 2$ and for variable frequency detuning δ. For both plots the oscillators are each driven by a time-harmonic force with equal frequency ω and amplitude per unit mass F. In (a) the two driving forces have equal phase ($F_1 = F_2$), while in (b) they are π-dephased ($F_1 = -F_2$).

Now we examine a feature commonly associated with strong coupling: avoided resonance crossing (ARC). An ARC arises when two resonances approach, and then repel, each other in frequency as some parameter is varied. For driven CHOs, this parameter can be the uncoupled eigenfrequency detuning $\delta = \omega_2 - \omega_1$. We illustrate the ARC phenomenon in figure 4 by calculating the dissipated power P_t as a function of the driving frequency ω and of the detuning parameter δ. The driven frequency is referenced to $\omega_0 = \omega_1$ for convenience. The losses of both oscillators are constant: $\gamma = 10^{-3}\omega_0$. Figure 4(a) shows results for $\Omega^2/\omega_0\gamma = 1$, and figure 4(b) corresponds to $\Omega^2/\omega_0\gamma = 2$. The two resonances that anti-cross near zero detuning ($\delta = 0$) constitute the ARC, and their splitting at $\delta = 0$ is the so-called Rabi splitting. In figure 4(a) we observe that for $|\delta/\gamma| \gtrsim 1$ the spectrum is dominated by a single resonance depending only weakly on δ. This is essentially the driven oscillator resonance. Since the CHOs are at the aforementioned smooth boundary between weak and strong coupling, a detuning of one linewidth is sufficient to practically vanish the influence of the second oscillator on the driven one. This changes for a stronger coupling strength as in figure 4(b). Notice in figure 4(b) that two resonances well separated in frequency seem to approach, but then repel, each other as δ passes through zero; this is a clear ARC. The resonances in figure 4(b) also deviate more from the uncoupled oscillator eigenfrequencies for a given δ than their counterparts in figure 4(a); this is expected due to the stronger coupling strength in figure 4(b).

ARC is a sufficient but not a necessary signature of strong coupling. The CHO response depends on the match between the driving force and the eigenmodes of the system. When only one oscillator is directly driven, ARCs are observed because both the symmetric and anti-symmetric modes can be excited with equal strength. This is no longer the case when both oscillators are directly driven and their relative phase is thereby imposed by the driving force. For example, consider the case where the two forces have equal amplitude and frequency. Thus, $F\mathrm{e}^{-\mathrm{i}\omega t+\phi}$ is included in the second row of the right-most term in equations (6) and (7). We present the case $\phi = 0$ in figure 5(a), and $\phi = \pi$ in figure 5(b). The lower branch is excited much more strongly in figure 5(a), while the opposite is true in figure 5(b). At $\delta = 0$ each driving scheme excites one resonance only, corresponding to the symmetric mode in figure 5(a) and to the anti-symmetric mode in figure 5(b). For $\delta \neq 0$ each oscillator supports symmetric and anti-symmetric modes at slightly different frequencies. Consequently, the net driving force no longer matches any one of the eigenmodes perfectly. Notice that the upper

resonance branch is progressively, although weakly, excited as $|\delta|$ increases in figure 5(a). A similar effect occurs for the lower resonance branch in figure 5(b).

Our spectral analysis has focused on a single observable—the total dissipated power. However, several experiments have been interpreted through a fit of the dissipated power by one oscillator only [10, 11, 37], or the CHO eigenvalues [26, 28]. A clear-cut distinction between weak and strong coupling is more difficult in such cases. The response of the two oscillators can in fact be pronouncedly different near the boundary between weak and strong coupling [37]. Studies of strong light-matter coupling have shown that the observable frequency splitting depends on how the system is probed, e.g. transmission, reflection, or absorption [38, 39]. The emission spectrum can also display a different frequency splitting [27]. Therefore, relating an observable in experiments with its counterpart in a fitted CHO model requires careful consideration. In this sense, the total dissipated power by the experimental and CHO model systems seem like a good figure of merit to demonstrate energy transfer between oscillators. While it may not always be easy to experimentally measure it, analysing the total dissipated power will likely lead to a more faithful mapping of the coupling regime of a system. Reference [27] illustrates a similar approach for a nanophotonic system. Reference [39] presents an interesting molecule-cavity system which can be actively tuned in and out of the strong coupling regime; all relevant observables (including the dissipated power) were obtained therein. Finally [25], illustrates an interesting alternative approach. The authors of [25] deduce the coupling and loss rates of a molecule-nanoparticle system by analysing its scattering spectrum with a CHO model.

4. NHH of CHOs

In this section we map the CHO equations of motion to the two-state NHH. The NHH we derive is similar to the Hamiltonian of a two state perturbed system (as discussed in introductory quantum mechanics textbooks [40]), with the important difference that for the NHH the energy spectrum is complex. As we will see, the imaginary part of the energy is directly related to the losses, i.e. the fact that the oscillators are in contact with a reservoir (air) where they dissipate energy.

We start by inserting the ansatz $x_j(t) = x_j^0 \mathrm{e}^{-\mathrm{i}\omega t}$ in equation (1), and writing the equations in matrix form. Next, dividing the first row by $\omega_1 + \omega$ and the second row by $\omega_2 + \omega$, we get

$$\begin{bmatrix} \omega_1 - \omega - \dfrac{\mathrm{i}\gamma_1\omega}{(\omega_1+\omega)} & -\dfrac{\Omega^2}{(\omega_1+\omega)} \\ -\dfrac{\Omega^2}{(\omega_2+\omega)} & \omega_2 - \omega - \dfrac{\mathrm{i}\gamma_2\omega}{(\omega_2+\omega)} \end{bmatrix} \begin{bmatrix} x_1 \\ x_2 \end{bmatrix} = \begin{bmatrix} 0 \\ 0 \end{bmatrix}. \tag{8}$$

Since we are interested in the response of the system at or near resonance, we assume $|\omega - \omega_{1,2}| \ll \omega$. Under this approximation and defining $\bar{\omega} \approx (\omega + \omega_{1,2})/2$ as the mean frequency, equation (8) becomes

$$\begin{bmatrix} \omega_1 - \dfrac{\mathrm{i}\gamma_1}{2} - \omega & -\dfrac{\Omega^2}{2\bar{\omega}} \\ -\dfrac{\Omega^2}{2\bar{\omega}} & \omega_2 - \dfrac{\mathrm{i}\gamma_2}{2} - \omega \end{bmatrix} \begin{bmatrix} x_1 \\ x_2 \end{bmatrix} = \begin{bmatrix} 0 \\ 0 \end{bmatrix}. \tag{9}$$

Equation (9) has non-trivial solutions if the determinant of the left-most term vanishes. Hence, we need to solve the characteristic equation $|H - \omega I| = 0$, where I is the identity matrix and

$$H = \begin{bmatrix} \omega_1 - \dfrac{\mathrm{i}\gamma_1}{2} & g \\ g & \omega_2 - \dfrac{\mathrm{i}\gamma_2}{2} \end{bmatrix}, \tag{10}$$

with $g = -\frac{\Omega^2}{2\tilde{\omega}}$ the effective coupling constant.

Equation (10) defines, in units of $\hbar = 1$, the two-state NHH corresponding to the CHOs. Through diagonalization and a little bit of algebra, we can write the eigenvalues of the NHH in the following form

$$\omega_\pm = \tilde{\omega} \pm \frac{\Delta}{2}\sqrt{1 + \left(\frac{2g}{\Delta}\right)^2}, \tag{11}$$

where we have defined $\tilde{\omega} = (\omega_1 + \omega_2)/2 - \mathrm{i}(\gamma_1 + \gamma_2)/4$ as the average complex frequency of the bare states, and $\Delta = (\omega_1 - \omega_2) - \mathrm{i}(\gamma_1 - \gamma_2)/2$ as their complex detuning. Physically, the real and imaginary parts of $\omega_\pm$ are associated with the peak frequencies and linewidths of decay resonances, respectively. We will denote these as follows: $\omega_\pm = \omega'_\pm - \mathrm{i}\omega''_\pm/2$. For the particular case of a lossless ($\gamma_1 = \gamma_2 = 0$) degenerate ($\omega_1 = \omega_2$) system, the eigenvalues (energies given our convention $\hbar = 1$) in equation (11) are those predicted by first-order time-independent degenerate perturbation theory [40]. They constitute the spectrum of a Hermitian Hamiltonian describing a conservative two-state quantum system under the influence of a perturbation with a strength proportional to g.

The mapping of the classical equations of motion of CHOs to a NHH sheds light on a connection between the physics of first order perturbation theory and coupled oscillators. This quantum-classical correspondence suggests that allowing Hamiltonians to be non-Hermitian in quantum mechanics amounts to allowing oscillators to be damped in classical mechanics. While the latter is common practice at the undergradaute level, the former is currently not. Since the non-Hermitian framework is becoming increasingly relevant at various fronts of physics [29–34], the present discussion conveys a simple approach through which advanced undergraduates or graduate students can be introduced to this topic.

Let us now analyse several of the general properties of the complex eigenfrequencies $\omega_\pm$. We do this through analytical inspection of equation (11). Taylor expanding the square root term at $\frac{2g}{\Delta} = 0$ yields

$$\omega_\pm \approx \tilde{\omega} \pm \frac{\Delta}{2}\left(1 + \left(\frac{2g}{\Delta}\right)^2 - \left(\frac{2g}{\Delta}\right)^4 \ldots\right). \tag{12}$$

Retaining only the leading term yields the frequencies of the bare states, i.e. $\omega_\pm = \tilde{\omega} \pm \Delta/2$. It follows that the influence of the coupling constant g on $\omega_\pm$ is negligible, or weak, as $\Delta \to \infty$.

We also recognize from equation (11) that the square root term is singular at $2g/\Delta = \pm\mathrm{i}$. The existence of this pole in the complex Δ plane implies that the perturbation series of $\omega_\pm$ in powers of $2g/\Delta$ converges inside a disk of radius $|2g/\Delta| = 1$. For $|2g/\Delta| \geqslant 1$, $\omega_\pm$ can not be analytically calculated by considering $2g/\Delta$ as a perturbation. This non-perturbative regime is therefore known as the strong coupling regime.

There are two important differences between the above definition of strong coupling and the one discussed in previous sections. Firstly, under the criterion derived in the present section, the ratio of the coupling constant to the individual loss rates or their sum imposes no restriction in defining the strong coupling regime. Secondly, the boundary between weak and strong coupling as determined by the perturbative or non-perturbative character of the

parameter $|2g/\Delta|$ is sharp. This sharpness is determined by the existence of a pole in the complex plane. In previous sections, energy exchange cycles and/or frequency splitting appeared smoothly as the parameter $\Omega^2/\omega_0\gamma$ increased above unity.

Next we illustrate the general behaviour of $\omega_\pm$ in the complex Δ plane. For brevity, we define $\Delta' = \omega_1 - \omega_2$ and $\Delta'' = (\gamma_1 - \gamma_2)/2$ as the real and imaginary parts of the complex detuning $\Delta = \Delta' - \mathrm{i}\Delta''$. The real part of $\omega_\pm$ is plotted in figure 6(a), and the imaginary part of $\omega_\pm$ is plotted in figure 6(b). All quantities in figure 6 are divided by $2g$ to render all axes dimensionless.

Figure 6 shows $\omega'_\pm$ and $\omega''_\pm$ in the complex plane. Interestingly, at $\Delta''/2g = \pm 1$ and $\Delta' = 0$ both the real and imaginary parts of ω_+ and ω_- coalesce. This is the so-called EP at the heart of non-Hermitian quantum mechanics [29]. The EP defines the boundary between strong and weak coupling. In contrast with a 2×2 Hermitian Hamiltonian involving purely real detuning ($\Delta'' = 0$), figure 6 shows that the eigenvalues of the NHH are analytic continuations of each other via the EP. Thus, by continuously varying Δ one energy level of the system is transformed into another.

To visualize the EP and its vicinity more clearly, we plot in figures 7(a) and (b) cuts of figures 6(a) and (b), respectively. In both panels we plot $\omega_\pm$ as a function $\Delta'/2g$ for three different values of $\Delta''/2g$. The blue dashed lines correspond to $\Delta''/2g = 0.9$, the black solid lines correspond to $\Delta''/2g = 1$, and the red dashed–dotted lines correspond to $\Delta''/2g = 1.1$. The blue dashed and red dashed–dotted lines illustrate the general structure of the NHH spectrum: level crossings imply anti-crossings of the corresponding resonance linewidths and vice versa [41]. However, at the EP both real and imaginary parts cross (black solid lines). There are various other fascinating aspects of the EP; we refer to Moiseyev for further details [29].

5. Concluding remarks

In section 2 we discussed the existence of two dynamical regimes based on the presence or absence of at least one cycle of energy exchange between CHOs. A single cycle of energy exchange corresponds to an observable resonance frequency splitting in the time-integrated power spectrum. Similarly, in section 3 we showed that the steady-state response of a driven CHO system displays an identical frequency splitting and an ARC under the same condition: $\Omega^2/\omega_0\gamma \gtrsim 1$. For both the dynamics and the steady-state response, the transition from weak to strong coupling as $\Omega^2/\omega_0\gamma$ increases above unity is smooth.

In section 4 we mapped the CHO equations of motion to the two-state NHH. Therein, we found that strong coupling corresponds to $|2g/\Delta| \geqslant 1$, with g the coupling constant and Δ the complex detuning between the bare states. This condition is based on the analytic properties of the NHH eigenvalues (energies) as a series in powers of $2g/\Delta$. In particular, weak and strong coupling are the regimes for which $2g/\Delta$ is perturbative or not, respectively. The distinction in this case is sharp; it is based on the presence of a pole in the complex plane.

The two criteria for strong coupling we discussed ($\Omega^2/\omega_0\gamma \gtrsim 1$ and $2g/\Delta \geqslant 1$) give the same result for many systems deep in the strong or weak coupling regimes. However, we have seen that certain systems can comply with one criterion but not the other. Firstly, in figure 2(a) we presented a system for which $\Omega^2/\omega_0\gamma < 1$ and $|2g/\Delta| \gg 1$, thereby complying with the second condition for strong coupling without displaying energy exchange cycles. Next, in figures 3(a) and (b) we considered systems with unequal eigenfrequencies and loss rates, respectively. The former sustained multiple (incomplete) energy exchange cycles, while the latter showed a single cycle of energy exchange. Therefore, while both systems in

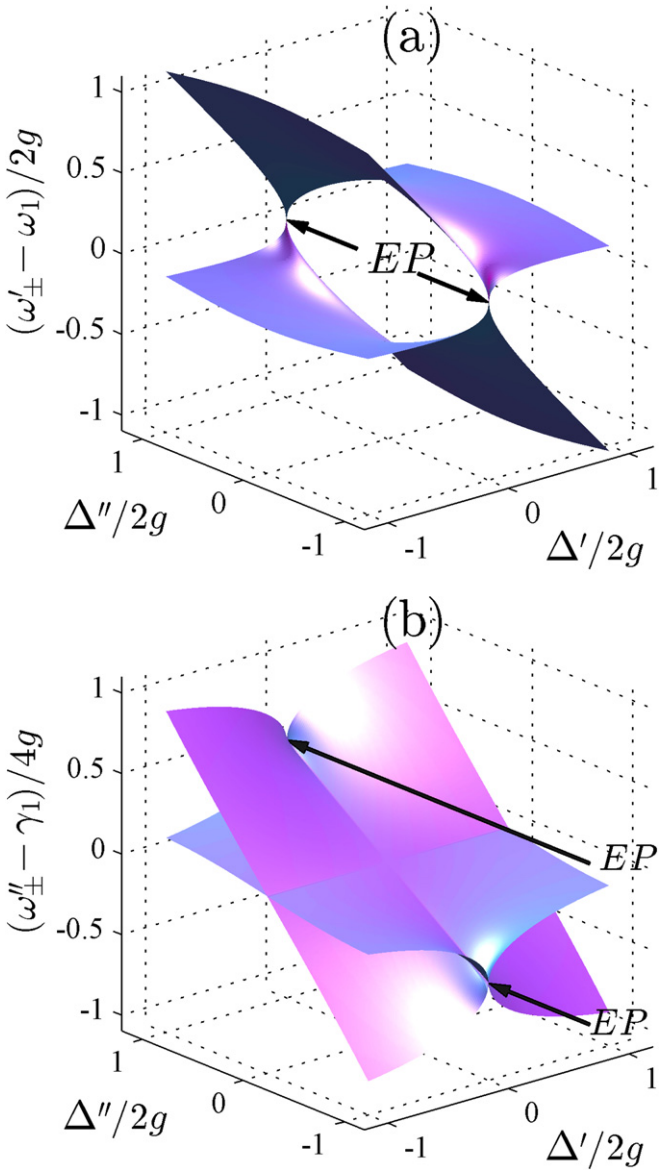

Figure 6. (a) Real and (b) imaginary parts of the non-Hermitian Hamiltonian eigenvalues plotted in the complex detuning plane. $\Delta' = \omega_1 - \omega_2$ is the real detuning and $\Delta'' = (\gamma_1 - \gamma_2)/2$ is the imaginary detuning. All quantities are divided by $2g$, with g the coupling constant, such that all axes are dimensionless. The exceptional points (EP) are indicated by the arrows.

figure 3 display energy exchange cycles, the condition $|2g/\Delta| \geqslant 1$ is not fulfilled. In view of these results, it is clear that the two definitions of strong coupling can not in general be used interchangeably. An anti-crossing of real eigenvalues does not imply energy exchange cycles or ARCs and vice versa.

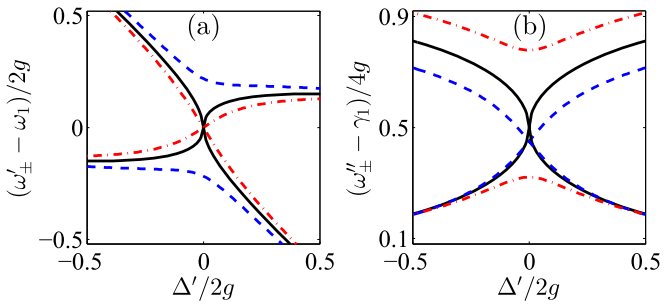

Figure 7. (a) and (b) are cuts of figures 6(a) and (b), respectively, at different values of $\Delta''/2g$. $\Delta''/2g = 1$ for the black solid lines , $\Delta''/2g = 0.9$ for the blue dashed lines, and $\Delta''/2g = 1.1$ for the red dashed–dotted lines. The exceptional point is at $\Delta''/2g = 1$ and $\Delta'/2g = 0$, where both real and imaginary parts of $\omega_\pm$ cross.

Understanding the physical differences associated with the distinct criteria for strong coupling is especially critical in studies of energy transfer. For example, the authors of [26] plotted calculated eigenvalues on top of measured reflectivity data in order to quantify energy transfer between molecules and a metallic structure. Interestingly, for some data sets the eigenvalues anti-cross while the measurements display single, at most weakly perturbed, resonance. Energy transfer is largely overwhelmed by dissipation in such cases (no energy exchange cycles). Another interesting example of how the model and approach employed can lead to significantly different conclusions transpires from comparing [25] with [42]. In [25] the authors observe a modest, but well-visible, ARC, and they conclude that they only approach but not fully reach the strong coupling regime. In contrast, in [42] a smaller frequency splitting, which is well below the largest resonance linewidth, is observed. Nevertheless, the authors claim to observe the strong coupling regime based on the anti-crossing of the real part of the resonance energy (eigenvalue) [42]. These two different interpretations, here taken as an example, are likely due to the use of different models and approaches. These examples illustrate why it is relevant to look at each system in different ways, and to raise awareness about the physical effects defining the boundary between weak and strong coupling in different formalisms.

Finally, it is worth mentioning that while a classical analog to strong coupling based on CHOs was presented in [3], the analogy relied on the anti-crossing of the eigenvalues of a lossless system. However, lossless systems can not in general define a boundary between weak and strong coupling. Every lossless system tuned in resonance is ‘strongly coupled’ for any nonzero energy exchange rate. It is only through the inclusion of losses and the departure from the Hermitian framework that the different features of weak and strong coupling in the classical and quantum descriptions can be recognized. Students can be introduced to all of these features, and to the key ideas of the non-Hermitian quantum framework, through mechanical models of CHOs or through their electrical counterparts which have proven successful in undergraduate laboratories worldwide [7, 14, 16].

Acknowledgments

I am grateful to J Gómez Rivas, F Koenderink, A Amo, J Bloch, S Mann, and T Coenen for stimulating discussions. I thank the Laboratoire de Photonique et Nanostructures, CNRS, where part of this work was completed. I acknowledge support from a Marie Curie Individual

Fellowship. This work was supported by the Netherlands Foundation for Fundamental Research on Matter (FOM) and the Netherlands Organization for Scientific Research (NWO), and is part of an industrial partnership program between Philips and FOM.

References

[1] Leggett A J, Chakravarty S, Dorsey A T, Fisher M P A, Garg A and Zwerger W 1987 Dynamics of the dissipative two-state system *Rev. Mod. Phys.* **59** 1–85
[2] Dragoman D and Dragoman M 2014 *Quantum-Classical Analogies* (*The Frontiers Collection*) (Berlin: Springer)
[3] Novotny L 2010 Strong coupling, energy splitting, and level crossings: a classical perspective *Am. J. Phys.* **78** 1199–202
[4] Törmä P and Barnes W L 2015 Strong coupling between surface plasmon polaritons and emitters: a review *Rep. Prog. Phys.* **78** 013901
[5] Andreani L C 2013 Exciton-polaritons in bulk semiconductors and in confined electron and photon systems *Strong Light-Matter Coupling* (Singapore: World Scientific) ch 2, pp 37–82
[6] Laussy F P, del Valle E and Tejedor C 2009 Luminescence spectra of quantum dots in microcavities: I. Bosons *Phys. Rev.* B **79** 235325
[7] Alzar C L G, Martinez M A G and Nussenzveig P 2002 Classical analog of electromagnetically induced transparency *Am. J. Phys.* **70** 37–41
[8] Joe Y S, Satanin A M and Kim C S 2006 Classical analogy of Fano resonances *Phys. Scr.* **74** 259
[9] Shore B W, Gromovyy M V, Yatsenko L P and Romanenko V I 2009 Simple mechanical analogs of rapid adiabatic passage in atomic physics *Am. J. Phys.* **77** 1183
[10] Liu N, Langguth L, Weiss T, Kästel J, Fleischhauer M, Pfau T and Giessen H 2009 Plasmonic analogue of electromagnetically induced transparency at the Drude damping limit *Nat. Mater.* **8** 758–62
[11] Mukherjee S, Sobhani H, Lassiter J B, Bardhan R, Nordlander P and Halas N J 2010 Fanoshells: nanoparticles with built-in Fano resonances *Nano Lett.* **10** 2694–701
[12] Miroshnichenko A E, Flach S and Kivshar Y S 2010 Fano resonances in nanoscale structures *Rev. Mod. Phys.* **82** 2257–98
[13] Shore B W 2011 *Manipulating Quantum Structures Using Laser Pulses* (Cambridge: Cambridge University Press)
[14] Harden J, Joshi A and Serna J D 2011 Demonstration of double EIT using coupled harmonic oscillators and RLC circuits *Eur. J. Phys.* **32** 541
[15] Tassin P, Zhang L, Zhao R, Jain A, Koschny T and Soukoulis C M 2012 Electromagnetically induced transparency and absorption in metamaterials: the radiating two-oscillator model and its experimental confirmation *Phys. Rev. Lett.* **109** 187401
[16] Satpathy S, Roy A and Mohapatra A 2012 Fano interference in classical oscillators *Eur. J. Phys.* **33** 863
[17] Briggs J S and Eisfeld A 2011 Equivalence of quantum and classical coherence in electronic energy transfer *Phys. Rev.* E **83** 051911
[18] Briggs J S and Eisfeld A 2012 Coherent quantum states from classical oscillator amplitudes *Phys. Rev.* A **85** 052111
[19] Briggs J S and Eisfeld A 2013 Quantum dynamics simulation with classical oscillators *Phys. Rev.* A **88** 062104
[20] Bender C M, Gianfreda M, Özdemir Şahin K, Peng B and Yang L 2013 Twofold transition in $\mathcal{PT}$-symmetric coupled oscillators *Phys. Rev.* A **88** 062111
[21] Frimmer M and Novotny L 2014 The classical Bloch equations *Am. J. Phys.* **82** 947–54
[22] Lidzey D G, Bradley D D C, Skolnick M S, Virgili T, Walker S and Whittaker D M 1998 Strong exciton-photon coupling in an organic semiconductor microcavity *Nature* **395** 53–5
[23] Groblacher S, Hammerer K, Vanner M R and Aspelmeyer M 2009 Observation of strong coupling between a micromechanical resonator and an optical cavity field *Nature* **460** 724–7
[24] Verhagen E, Deleglise S, Weis S, Schliesser A and Kippenberg T J 2012 Quantum-coherent coupling of a mechanical oscillator to an optical cavity mode *Nature* **482** 63–7
[25] Zengin G, Johansson G, Johansson P, Antosiewicz T J, Käll M and Shegai T 2013 Approaching the strong coupling limit in single plasmonic nanorods interacting with j-aggregates *Sci. Rep.* **3** 3074

[26] Koponen M A, Hohenester U, Hakala T K and Toppari J J 2013 Absence of mutual polariton scattering for strongly coupled surface plasmon polaritons and dye molecules with a large stokes shift *Phys. Rev.* B **88** 085425
[27] Rodriguez S R K, Chen Y T, Steinbusch T P, Verschuuren M A, Koenderink A F and Rivas J G 2014 From weak to strong coupling of localized surface plasmons to guided modes in a luminescent slab *Phys. Rev.* B **90** 235406
[28] Liu X, Galfsky T, Sun Z, Xia F, Erh-chen L, Yi-Hsien L, Kéna-Cohen S and Menon V M 2015 Strong light-matter coupling in two-dimensional atomic crystals *Nat. Photon.* **9** 30–4
[29] Moiseyev N 2011 *Non-Hermitian Quantum Mechanics* (Cambridge: Cambridge University Press)
[30] Philipp M, von Brentano P, Pascovici G and Richter A 2000 Frequency and width crossing of two interacting resonances in a microwave cavity *Phys. Rev.* E **62** 1922–6
[31] Dembowski C, Gräf H-D, Harney H L, Heine A, Heiss W D, Rehfeld H and Richter A 2001 Experimental observation of the topological structure of exceptional points *Phys. Rev. Lett.* **86** 787–90
[32] Heiss W D 2012 The physics of exceptional points *J. Phys. A: Math. Theor.* **45** 444016
[33] Rüter C E, Makris K G, El-Ganainy R, Christodoulides D N, Segev M and Kip D 2010 Observation of parity-time symmetry in optics *Nat. Phys.* **6** 192–5
[34] Peng B, Özdemir Şahin K, Lei F, Monifi F, Gianfreda M, Long G L, Fan S, Nori F, Bender C M and Yang L 2014 Parity-time-symmetric whispering-gallery microcavities *Nat. Phys.* **10** 394–8
[35] Shore B W and Vitanov N V 2006 Overdamping of coherently driven quantum systems *Contemp. Phys.* **47** 341–62
[36] Agarwal G S 1985 Vacuum-field Rabi oscillations of atoms in a cavity *J. Opt. Soc. Am.* B **2** 480–5
[37] Rodriguez S R K, Murai S, Verschuuren M A and Gómez Rivas J 2012 Light-emitting waveguide-plasmon polaritons *Phys. Rev. Lett.* **109** 166803
[38] Savona V, Andreani L C, Schwendimann P and Quattropani A 1995 Quantum well excitons in semiconductor microcavities: unified treatment of weak and strong coupling regimes *Solid State Commun.* **93** 733–9
[39] Schwartz T, Hutchison J A, Genet C and Ebbesen T W 2011 Reversible switching of ultrastrong light-molecule coupling *Phys. Rev. Lett.* **106** 196405
[40] Griffiths D J 2005 *Introduction to Quantum Mechanics* (Englewood Cliffs, NJ: Prentice-Hall) Pearson International edition
[41] Heiss W D 2000 Repulsion of resonance states and exceptional points *Phys. Rev.* E **61** 929–32
[42] Anne-Laure B, Antoine P, Alessandro V, Alexandre B, Pierre-Michel A and Renaud B 2013 Reversible strong coupling in silver nanoparticle arrays using photochromic molecules *Nano Lett.* **13** 282–6